

Star Formation Histories of Dwarf Lenticular Galaxies

Hong Bae Ann¹* and Mira Seo¹

¹Department of Earth Sciences, Pusan National University, 46241, Busan, Korea

Accepted XXX. Received YYY; in original form ZZZ

ABSTRACT

We present the mean star formation histories (SFHs) of 148 dwarf lenticular galaxies (dS0s) derived from SDSS spectra. The SFHs of dS0s are characterized by multiple bursts of star formation, including an initial burst at a lookback time of ~ 14 Gyr for most galaxies. Stars formed during the first star-forming phase which ends at a lookback time of 6.3 Gyr primarily consist of old, metal-poor ($Z=0.0004$) stars, contributing to $\sim 60\%$ of the stellar mass and $\sim 30\%$ of the luminosity. The almost absence of extremely metal poor ($Z=0.0001$) stars seems to be due to pre-enrichment during the re-ionization era. Star formation gradually decreases during this initial period. In contrast, during the second period of star formation, there is an increase in star formation activity, peaking at a lookback time of 2.5 Gyr before declining again. Most moderately old stellar populations with intermediate metallicity were formed during this phase. We observe a strong dependence of SFHs on the mass and u-r color of dS0 galaxies but no significant dependence on morphological properties such as the presence or absence of outer spiral arms and nucleation. The star formation history of dS0 galaxies shares many similarities with that of dE galaxies, and many of them are believed to have originated from late-type galaxies.

galaxies.

Key words: galaxies: dwarfs – galaxies: formation – galaxies: evolution – galaxies: star formation

1 INTRODUCTION

Dwarf lenticular galaxies (dS0s) are early-type dwarf galaxies whose morphology is similar to dwarf elliptical galaxies (dEs), but they possess a bulge/lens-like component in the inner regions. They were introduced by [Sandage & Binggeli \(1984\)](#) as a class of dwarf galaxies in the Virgo Cluster. [Binggeli & Cameron \(1991\)](#) conducted a detailed examination of the morphologies of dS0s, using 20 dS0s in the Virgo cluster. Their study revealed a variety of disc features present in the two-dimensional images of dS0s. The surface brightness profiles of dS0s resemble those of dEs, which are well fitted by exponential profiles or King profiles, displaying an excess of light in the central regions ([Binggeli & Cameron 1991, 1993](#)). The similarity in surface brightness profiles of dEs and dS0s has raised questions regarding whether dS0s truly represent a distinct class of dwarf galaxies (e.g., [Reyden et al. 1999](#)), leading to some researchers treating dS0s as a subclass of dEs (e.g., [Barazza et al. 2003](#)).

However, if we accept the definition of dE and dS0 galaxies as introduced by [Sandage & Binggeli \(1984\)](#), it appears reasonable to differentiate dS0s from dEs based on their surface brightness profiles, as dS0s exhibit multiple components—one for the inner regions and another for the outer regions. The surface brightness profile of the inner component is most ac-

curately described by the Sérsic profile ([Sérsic 1968](#)) while that of the outer component conforms to an exponential profile. The inner component is generally regarded as a lens ([Buta 2013](#)), whereas the outer component is seen as a disc. Leveraging this characteristic of dS0s' surface brightness, [Aguerri et al. \(2005\)](#) classified the early-type dwarfs in the Coma cluster into dEs and dS0s. They considered a galaxy to be a dE if a single component, the Sérsic profile, provided a good fit to the observed surface brightness profile. Conversely, they classified it as a dS0 if two components, Sérsic + exponential, were necessary to meet the constraint imposed on the residuals. Their method resulted in the identification of 29 dS0s and 55 dEs. A more comprehensive profile analysis was conducted by [Janz et al. \(2012, 2014\)](#) using GALFIT ([Peng et al. 2010](#)), a two-dimensional decomposition tool, on 121 early-type dwarfs in the Virgo cluster observed in the near-infrared H -band. Only approximately one-third of the sample galaxies were found to possess a single component, while the majority of the 121 early-type dwarfs exhibited two or more components, including lenses and bars. Although they did not specify the morphological types of multi-component galaxies, a substantial proportion of multi-component dwarfs are likely to be dS0s.

Despite the examples of dS0s provided by [Binggeli & Cameron \(1991\)](#) and the effectiveness of two-component models demonstrated by [Aguerri et al. \(2005\)](#), the ongoing debate revolves around whether dS0 should be considered a distinct,

* E-mail: hbann@pusan.ac.kr

coequal category among early-type dwarfs. Many authors opt to refrain from explicitly designating dS0 as a separate class of early-type dwarf galaxies, instead employing dEs to encompass both dwarf elliptical galaxies and subsuming dSphs and dS0s within this category (e.g., Barazza et al. 2003). This tendency arises partly due to the limited number of dS0s in comparison to dEs, especially within the Virgo cluster, and the presence of disc features such as spiral arms, bars, and lenses observed in both dEs and dS0s (Jerjen et al. 2000, 2001; Barazza et al. 2002; Rijcke et al. 2003; Graham & Guzman 2003; Graham et al. 2003; Ferrarese et al. 2006; Lisker et al. 2006; Lisker 2009; Janz et al. 2012; Penny et al. 2014; Graham et al. 2017).

In light of these considerations, Lisker et al. (2006, 2007) made a distinction among early-type dwarf galaxies based on the presence or absence of embedded disc features, rather than isolating dS0 as a separate category. Galaxies devoid of disc features were categorized as dE, while those exhibiting such features were designated as dE(di).

The fraction of embedded disc features in dEs is no lower than that observed in dS0s (Seo & Ann 2022). These embedded disc features are predominantly found in the brighter early-type dwarfs. The absence of disc features in the faint early-type dwarfs within the Virgo cluster aligns with the lack of such features in dSphs as well (Seo & Ann 2022). While the dEs classified by Binggeli et al. (1985) encompass dSphs, which are generally faint early-type dwarfs, Ann et al. (2015) includes dSph as a class of early-type dwarfs in the morphology classification of galaxies in the local universe observed by the Sloan Digital Sky Survey (SDSS) (York et al. 2000).

It appears advisable to maintain the classification of dS0, even when employing dE(di) for other purposes, because the presence of embedded disc features is not unique to dS0s. Rather, the two-component nature of dS0s is an inherent characteristic of the dS0 type. Furthermore, the existence of spiral arms in the outer disc of certain dS0s represents a distinctive feature of this class. Ann et al. (2015) classified such cases as dS0_p, signifying peculiar dS0s.

The importance of morphological classification for dS0 galaxies has been reaffirmed in recent visual galaxy classification efforts, exemplified by projects such as the Extended Virgo Cluster Catalog (Kim et al. 2014, hereafter EVCC) and the catalog of visually classified galaxies in the local universe within $z = 0.01$ (Ann et al. 2015, hereafter CVC). Notably, the number of dS0s in the EVCC is nearly double that of the Virgo Cluster Catalog (VCC), while the count of dEs remains relatively stable. This increase in the number of dS0s in the EVCC primarily results from reclassifying certain dEs from the VCC as dS0s in the EVCC. Additionally, a slight decrease in the count of dEs in the EVCC is due to the reclassification of some dEs from the VCC as E, S0, and Sa galaxies.

In the Virgo cluster, the count of dS0s is less than one-tenth of the count of dEs (Binggeli & Cameron 1991; Kim et al. 2014). In contrast, in the local universe, the number of dS0s is approximately 60% of the number of dEs (Ann et al. 2015). One reason for the significant difference in the ratio of dEs to dS0s between the Virgo cluster and the local universe is that dSphs are classified as dEs in the VCC by Binggeli et al. (1985) and in the EVCC by Kim et al. (2014), whereas dSphs are categorized as a separate morphological type in the CVC. Most of the faint dEs in the VCC and EVCC are classified as dSphs in the CVC.

The origin of dS0s is a subject of particular interest. Similar to dEs, there are two plausible scenarios for their formation: one related to their primordial origins and the other involving transformation processes. If dS0s are indeed transformed from late-type galaxies, the conversion of gas-rich disc galaxies into gas-poor early-type dwarfs likely involves two distinct phases. The initial phase entails gas removal, while the subsequent stage includes processes such as tidal heating and harassment. Given that a significant portion of dS0s are found in group and cluster environments (Makarov & Karachentsev 2011; Ann 2017), these transformation mechanisms may involve ram pressure stripping (Gunn & Gott 1972) and galaxy harassment (Moore et al. 1996, 1998).

In contrast, Boselli et al. (2008) and Steyrlithner et al. (2020) have reported that the transformation of late-type galaxies into early-type dwarfs can be achieved solely through ram pressure stripping, while Chilingarian et al. (2009) suggested the possibility of major/minor mergers playing a role. The morphological transformation from late-type galaxies to early-type dwarfs is feasible because ram pressure not only removes cold gas but also compresses it, leading to star formation. The grand-design spiral arms observed in unsharp masked images of some early-type galaxies (e.g., Lisker et al. 2006) are believed to form in the gas compressed by ram pressure. The disc features, including arms, bars, lenses, and clumps, seen in the residual images of early-type dwarfs, especially dS0s, could result from star formation driven by ram pressure. Ram pressure has the effect of heating a thin stellar disc, turning it into a thicker one by removing the gas potential (Smith et al. 2012). Additionally, gas clouds pushed out of the disc by ram pressure but still gravitationally bound may fall back in and contribute to star formation in the thick disc (Steyrlithner et al. 2020; Boselli et al. 2022).

Conversely, the hypothesis of a primordial origin for dS0s remains a viable one, supported by the fact that approximately 5% of them exist as isolated galaxies, unaffected by environmental factors that could potentially alter their morphology. However, recent analyses of the star formation histories (SFHs) of dEs and dSphs (Seo & Ann 2023), derived from SDSS spectra, have revealed that a significant fraction of dEs cannot be considered primordial objects, as they exhibit active periods of star formation around a lookback time of 2.5 Gyr, whereas the majority of dSphs are believed to be primordial objects. Since dS0s share many similarities with dEs, it is reasonable to expect that the SFHs of dS0s are similar to those of dEs.

There have been relatively few studies on the SFHs of dS0s, primarily due to the scarcity of dS0s within the Local Group (LG), where SFHs of dwarf galaxies can be derived using the Color-Magnitude Diagram (CMD) method (Tolstoy et al. 2009). The primary objective of this paper is to investigate the origin of dS0 galaxies by analyzing how their SFHs. It is well-established that stellar mass plays a pivotal role in driving star formation in galaxies, resulting in the earlier formation of stars in more massive galaxies compared to less massive ones (Cowie et al. 1996; Gavazzi et al. 2006; De Lucia et al. 2007; Sánchez-Blázquez 2009). The relationship between star formation rates (SFRs) and stellar mass is also well-documented (Brinchmann et al. 2004; Daddi et al. 2007; Noeske et al. 1997; Salim et al. 2007; Rodighiero et al. 2011; Sobral et al. 2014; Speagle et al. 2014).

The influence of the environment on the SFHs of galaxies

has been studied extensively for bright galaxies (Spitzer & Baade 1951; Oemler 1974; Dressler 1980; Kauffmann et al. 2004; Wang 2022; Pérez-Millán et al. 2023), as well as for early-type dwarfs, specifically dSphs and dEs (Seo & Ann 2023). In this research, we focus on the SFHs of dS0s, paying special attention to the dependence of the cumulative star formation histories (cSFHs) on the physical and morphological properties of dS0s, as well as their environment. To achieve this, we derive the stellar populations by applying the population synthesis code STARLIGHT (Cid Fernandes et al. 2005) to the spectra of these galaxies observed by the SDSS.

The structure of this paper is organized as follows. In Section 2, we outline the process of selecting sample galaxies and provide a brief overview of the method for analyzing spectra using STARLIGHT. Section 3 presents the SFHs of dS0s, focusing on luminosity and mass fractions. In Section 4, we present the cSFHs obtained from our analysis. Finally, in Section 5, we conclude the study by discussing our findings

2 DATA AND METHOD

2.1 Data

We utilized the SDSS spectra of 148 dS0 galaxies, all of which are listed in the CVCG. While the CVCG initially includes 154 dS0 galaxies, we were able to obtain spectra for 148 dS0s from the SDSS Data Release 7 (DR7). It's worth noting that the CVCG encompasses a total of 5,638 galaxies situated in the local universe. Furthermore, the CVCG is nearly complete for galaxies brighter than $r = 17.77$ in the regions covered by the SDSS. The detailed classification of dS0 galaxies was provided by Ann et al. (2015), who distinguished dS0s with spiral arm features as peculiar dS0s, and also differentiated between nucleated and non-nucleated dS0s. Among the 148 dS0 galaxies, 30 exhibit spiral arms in the outer regions, constituting roughly 20% of the dS0 population. Concerning nucleation, the number of nucleated dS0 galaxies is comparable to that of non-nucleated dS0s.

Figure 1 presents color images of four sample galaxies, with two belonging to dS0s without spiral arm features (upper row) and the other two to dS0s with spiral arm features in the outer regions (lower row). In the right panel of each pair, we show nucleated dS0s, while the left panel displays non-nucleated dS0s. A notable observation from these images is the presence of a lens-like component in the inner regions of the dS0s, which is a distinctive feature.

As illustrated in Figure 2, dS0s with spiral arm features appear slightly fainter compared to those without such features. It's worth mentioning that nearly all dS0s with spiral arm features are fainter than $M_r = -16$. Furthermore, the majority of dS0s are situated along the red sequence (Strateva et al. 2001), although there are some notable deviations. The significant dispersion in the $u - r$ colors among dS0s is likely attributed to the relatively large photometric errors in u -band magnitudes, especially for faint galaxies.

The SDSS spectra were captured using fibers with a diameter of 3 arcsec, positioned at the focal plane of the 2.5-meter telescope located at the Apache Point Observatory. The SDSS spectrograph incorporates 320 fibers, and the exposures lasted for 45 minutes or more, ensuring a fiducial

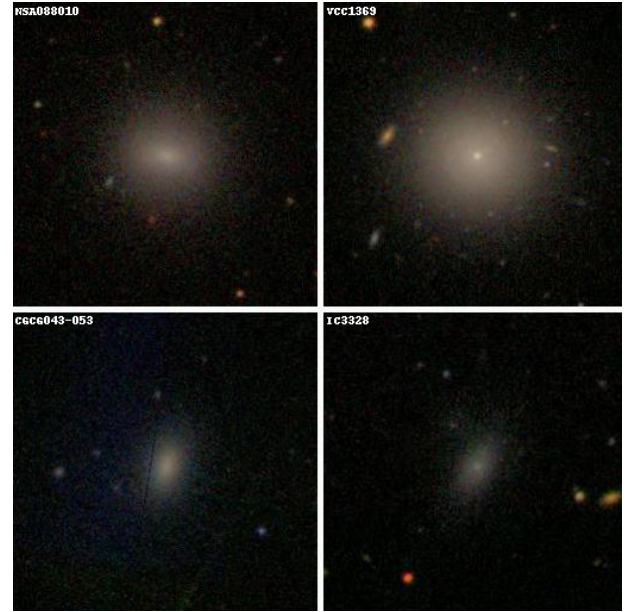


Figure 1. The SDSS color images of four dS0 galaxies: NSA 088010, VCC 1369, IC 3328, and CGCG 043-053, clock-wise from the upper left. The galaxies in the upper row are dS0s without spiral arms, while those in the lower row exhibit spiral arm features in the outer regions. The left panels correspond to non-nucleated dS0s, and the right panels depict nucleated dS0s. The box size in one dimension is ~ 50 arcsec. North is at the top, and East is to the left.

signal-to-noise ratio. The spectra encompass a wavelength range spanning from 3800 to 9200 Å, with an average spectral resolution of $\lambda/\Delta\lambda \sim 1800$. The wavelength and flux values have been calibrated using the pipeline developed by the SDSS team. We have also incorporated observational data from Ann et al. (2015), which includes information such as distance, luminosity (M_r), color ($u - r$), morphological type, as well as coordinates and redshift.

2.2 Method

We utilized the STARLIGHT code (Cid Fernandes et al. 2005) to analyze the SDSS spectra of 148 dS0s. STARLIGHT allows us to determine the most likely combination of stellar populations based on their ages and metallicities. The STARLIGHT code has been thoroughly documented by Cid Fernandes et al. (2004) and Cid Fernandes et al. (2005), and it has been applied in a number of studies including the recent studies such as Riffel et al. (2021) and Seo & Ann (2023).

STARLIGHT fits the observed spectrum by generating a model spectrum derived from population synthesis models based on simple stellar populations (SSPs) from Bruzual & Charlot (2003). These models incorporate six metallicities ($Z = 0.0001, 0.0004, 0.004, 0.008, 0.02$, and 0.05) and ages ranging from 1×10^5 to 2×10^{10} years to represent the spectral evolution of SSPs. The stellar populations encompass stars with lower and upper mass cut-offs of $m_L = 0.1M_\odot$ and $m_U = 100M_\odot$. Bruzual & Charlot (2003) utilized basic stellar evolutionary tracks from the Padova groups, complemented by the Geneva groups' data, along with the STELIB library (Le Borgne et al. 2003).

In the STARLIGHT framework, the model spectrum M_λ

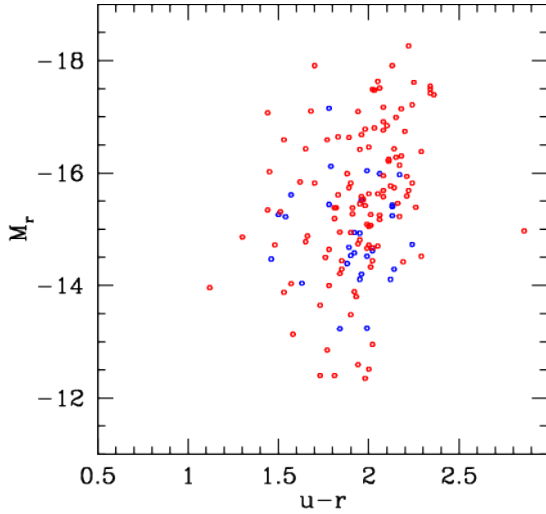


Figure 2. Color-magnitude diagram of dS0 galaxies. Galaxies with spiral arm features are represented by blue circles, while those without spiral arm features are represented by red circles.

is represented as

$$M_\lambda = M_{\lambda_0} \left(\sum_{j=1}^{N_*} x_j b_{j,\lambda} r_\lambda \right) \otimes G(v_*, \sigma_*) \quad (1)$$

where $b_{j,\lambda}$ is the j -th SSP spectrum normalized at λ_0 , $r_\lambda = 10^{-0.4(A_\lambda - A_{\lambda_0})}$, M_{λ_0} is the synthetic flux at the normalization wavelength λ_0 , and x_j is the fractional contribution of the SSP for j -th population that has age t_j and metallicity Z_j . The stellar motion projected on the line-of-sight is modeled by a Gaussian distribution (G) centered on the galaxy radial velocity v with velocity dispersion σ . Extinction due to foreground dust is taken into account using the V-band extinction A_V . The best fitting model is determined by selecting a model that minimizes the $\Xi^2 = \Sigma[(O_\lambda - M_\lambda)w_\lambda]^2$ where O_λ is observed spectrum and w_λ is the inverse of error applied (see [Cid Fernandes et al. \(2004\)](#) for a detailed description).

We resampled the observed spectrum with a sampling width of $\delta\lambda=1\text{\AA}$, after correcting the interstellar reddening and redshift following [Seo & Ann \(2023\)](#). In STARLIGHT, the luminosity fraction (x_j) and mass fraction (μ_j) for the j -th stellar population are divided into six stellar metallicities ($Z=0.0001, 0.0004, 0.004, 0.008, 0.02$, and 0.05). It assumes $[\alpha/\text{Fe}]=0$. The STARLIGHT output provides two mass fractions, μ_{ini} and μ_{cor} , which represent initial mass and mass corrected for the mass returned to the interstellar medium, respectively. We used the μ_{cor} for the mass fraction of stellar populations while we used the μ_{ini} to derive the star formation rates.

Figure 3 shows an example of population synthesis carried out using STARLIGHT. The model spectrum well represents the details of the observed spectrum of IC 3540 which is a dwarf lenticular galaxy in the Virgo cluster. The robustness of the stellar populations derived by STARLIGHT has been examined in previous works ([Magris et al. 2015](#); [Cid Fernandes 2018](#); [Seo & Ann 2023](#)). To assess its reliability, [Seo & Ann \(2023\)](#) conducted mock tests using STARLIGHT, where they generated mock spectra from model fluxes perturbed

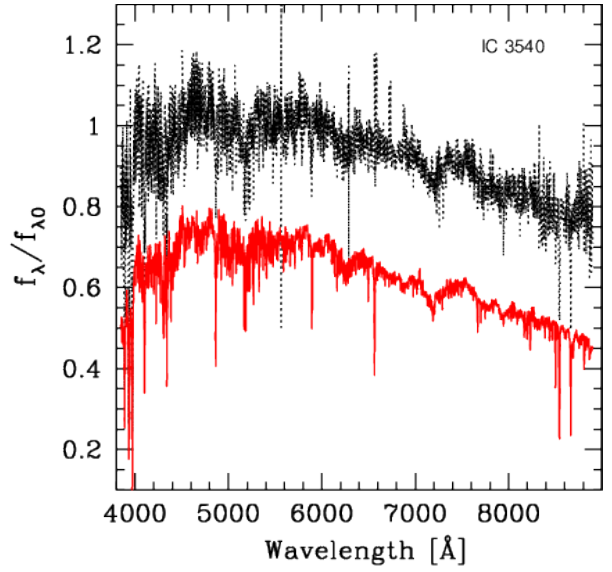


Figure 3. Normalized fluxes as a function of wavelength. The observed flux is plotted with a black line, and the synthesis flux is depicted with a red line. We have offset the synthesis flux by -0.3 for visibility. Flux is normalized by the flux at $\lambda = 4020\text{\AA}$.

by Gaussian noise levels proportional to $(S/N)^{-1}$. They observed that ages and metallicities of mock galaxies were well reproduced, except for spectra with $S/N = 5$. Here we present a comparison of the mean ages and metallicities derived from STARLIGHT and pPXF ([Cappellari & Emsellem 2004](#)). The mean ages and metallicities are calculated using luminosity-weighted values through the following equations,

$$\log t_* = \sum_{j=1}^{N_*} L_j \log t_j \quad (2)$$

$$Z = \sum_{j=1}^{N_*} L_j Z_j \quad (3)$$

where L_j is the fractional luminosity contribution of j -th population and $\log t_j$ and Z_j are its stellar age and metallicity, respectively. As shown in Figure 4, the two data sets show reasonable agreement which enforces the robustness of the methods applied if we treat them statistically.

3 STAR FORMATION HISTORY

3.1 Luminosity and Mass Fraction

Figure 5 presents the mean luminosity and mass fractions of the stellar populations as a function of stellar age for dS0 galaxies. We applied sigma clipping to exclude galaxies deviating by more than 3σ from the mean. The number of rejected galaxies accounts for less than $\sim 3\%$ of the entire sample. It is convenient to use lookback time (t_L) to describe the SFHs of galaxies. One prominent characteristic of the SFHs of dS0 galaxies is the presence of multiple bursts of star formation. The first period of active star formation commenced with an explosive burst at $\log(t_L) = 10.14$ and concluded at

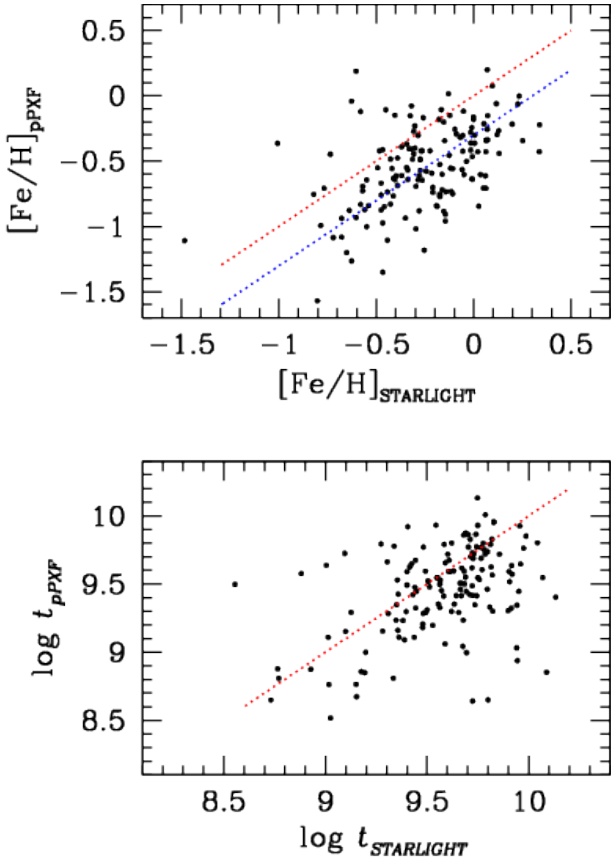


Figure 4. comparison of mean ages and metallicities between STARLIGHT and pPXF. We plot the one-to-one relation as red dotted lines. The best fitted relation between $[\text{Fe}/\text{H}]_{\text{pPXF}}$ and $[\text{Fe}/\text{H}]_{\text{STARLIGHT}}$

$\log(t_L) \approx 9.8$. There was a gradual decrease in star formation during this initial period. In contrast, the second period of active star formation exhibited a peak at $\log(t_L) \approx 9.4$ and extended from $\log(t_L) \approx 9.8$ to $\log(t_L) \approx 9.0$. Afterward, a brief quiescent phase followed. Subsequently, there was a resurgence of star formation activity at $\log(t_L) \approx 8$, albeit at significantly reduced intensity. This pattern, which includes a period of quenched star formation between $\log(t_L) \approx 9$ and $\log(t_L) \approx 8$, represents a common feature observed in the SFHs of early-type dwarf galaxies within the LG (Tolstoy et al. 2009).

It's worth noting that approximately 60% of the stellar mass was produced during the first period of star formation, and more than 99.8% of the stellar mass was produced by the end of the second period. Thus, concerning stellar mass, star formation virtually ceased at $\log(t_L) \approx 9$. However, in terms of luminosity, star formation continues until recently to produce young massive stars. The SFHs of dS0 galaxies exhibit striking similarities to the SFHs of dEs (Seo & Ann 2023). This suggests that there are commonalities in the star formation histories of these two classes of early-type dwarf galaxies.

While the general trend of star formation activity during the first period exhibits a gradual decrease, it is not strictly monotonic. There is a brief period of significantly reduced star formation immediately after the initial explosive star-

burst, followed by a slight increase that leads to a peak at $\log(t_L) = 10$. This second peak within the first period is comparable to the distinct peak at $\log(t_L) = 9.4$ in the second period.

In terms of luminosity fractions, the initial burst of dS0 galaxies which contributes $\sim 10\%$ of the present luminosity is much weaker than the strongest burst at $\log(t_L) = 9.4$ and the stars formed in the first period of star formation contribute $\sim 30\%$ of the present luminosity in total. However, we consider the first period as the primary phase of star formation because $\sim 60\%$ of the stellar mass was formed during this interval. Moreover, over 50% of the mass is contributed by stars older than approximately 10 Gyr. The oldest stars, which formed at $\log(t_L) \approx 10.14$, currently contribute roughly 25% of the total stellar mass and around 10% of the total luminosity. As described below, the oldest stars are predominantly metal-poor ($Z=0.0004$) stars.

After the second period of star formation, the general star formation behavior is characterized by a period of quenched star formation until $\log(t_L) \approx 8$, followed by increased star formation activity leading up to the present time. However, the total mass contribution by stars younger than approximately 0.1 Gyr is less than 5%. The near absence of star formation between $\log(t_L) \approx 9$ and $\log(t_L) \approx 8$ has resulted in the lack of intermediate-age stars older than approximately 0.1 Gyr. This feature, marked by highly suppressed star formation in intermediate-age stars, is also observed in some early-type dwarfs in the LG (Weisz et al. 2014a), as well as in dSphs and dEs in the local universe (Seo & Ann 2023). The suppression of star formation is believed to be caused by stellar feedback mechanisms such as supernova explosions and stellar winds. The cold gas within galaxies gets heated and is easily expelled into the halos of early-type dwarfs.

The resurgence of star formation around $\log(t_L) \approx 8$ is believed to be primarily influenced by the accretion of cold intergalactic medium (IGM). It contributes $\sim 5\%$ of the present luminosity and less than 0.2% of the total stellar mass. This hypothesis gains support from the observed metallicity of stars formed immediately following the period of quenched star formation, which can be accounted for by assuming the accretion of metal-free IGM, as elaborated below.

3.2 Metallicity Dependent Mass Fraction

Figure 6 shows the mean mass fractions of the stellar populations of 148 dS0s, divided into 6 metallicity groups, as a function of stellar age. As described above for the derivation of mean luminosity and mass fractions, we applied a sigma clipping method to exclude outliers. The stellar metallicities we used are $Z=0.0001$, $Z=0.0004$, $Z=0.004$, $Z=0.008$, $Z=0.02$, and $Z=0.05$. The most pronounced feature of the SFHs of dS0s is the lack of extremely metal-poor ($Z=0.0001$) stars formed at $\log(t_L) \gtrsim 10$. Among the stars formed at $\log(t_L) \gtrsim 10$, which contribute $\sim 50\%$ of the present stellar mass, more than $\sim 80\%$ of them are metal-poor and the rest have metallicities of $Z=0.004$, 0.008 , 0.02 , and 0.05 , each of which contributes $\sim 5\%$ at most. Stars formed from the initial burst at $\log(t_L) \approx 10.14$ are also mostly (80%) metal-poor stars. The absence of extremely metal-poor stars formed in the first and second periods of star formation is also observed in dSphs and dEs (Seo & Ann 2023) which is assumed to be due to pre-enrichment during the re-ionization era.

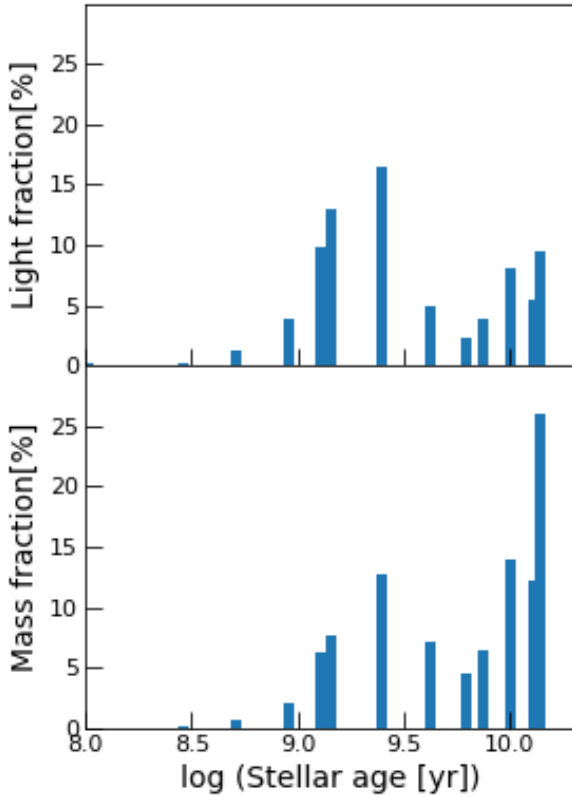


Figure 5. Mean luminosity and mass fractions as a function of stellar age for 148 dS0 galaxies. The upper panel shows the luminosity fraction, while the lower panel shows the mass fraction.

The chemical evolution of dS0 galaxies during the second period of star formation closely parallels that of dEs (Seo & Ann 2023). Specifically, it commences with intermediate metallicities ($Z=0.004$ and $Z=0.008$) and concludes with the emergence of extremely metal-rich stars. Within the second period of star formation, the predominant metallicity is the intermediate metallicity of $Z=0.008$, accounting for more than half of the stars formed during this phase. This high prevalence of stars with $Z=0.008$ is attributed to the rapid enrichment process in dS0 galaxies.

Due to this swift enrichment, extremely metal-rich stars are produced in the latter stages of the second period of star formation. In fact, all generations of stars formed during the first and second periods of star formation exhibit some extremely metal-rich stars, although their contribution to the current stellar mass is relatively small, with the exception of stars formed at $\log(t_L) \approx 9.1$.

The occurrence of a quenched period of star formation in dS0 galaxies could be attributed to the explosive starbursts that took place during the initial phase of star formation, which expelled the remaining gas into the galactic halo. Over time, this gas, retained within the halo of dS0 galaxies, eventually falls back and leads to star formation after a period of dormancy. Similar characteristics have been observed in dEs as well (Seo & Ann 2023).

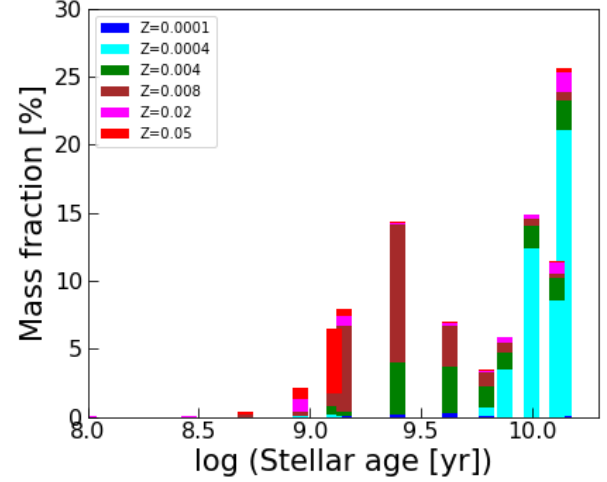


Figure 6. Mean mass fractions of stellar populations as a function of stellar age for 148 dS0 galaxies. The stellar populations are divided by their metallicities.

4 CUMULATIVE STAR FORMATION HISTORY

4.1 Mean cSFHs

As have seen in Figures 5 and 6, the mean SFH of dS0 galaxies varies significantly since the beginning of star formation at ~ 14 Gyr ago. To understand the mass assembly history of dS0 galaxies more clearly we examine the cumulative star formation histories (cSFHS) of dS0s in detail below. Here again, we examine the mean cSFH of dS0 galaxies rather than cSFH of individual galaxies because the cSFH of individual galaxy is very diverse. We derived a mean cSFH of dS0 galaxies by applying 3σ clipping. The mean cSFH could help in identifying overarching trends and patterns that apply broadly to this class of galaxies, shedding light on their evolutionary processes. For comparison with other early-type galaxies, dSphs and dEs which were studied by Seo & Ann (2023), we plotted the cSFHs of these types together in Figure 7.

The general behaviour of the cSFHs of dS0s is characterized by a rapid increase of cSFH due to bursts of star formation occurring at $\log(t_L) \gtrsim 10$, contributing to $\sim 50\%$ of the present stellar mass. Subsequently, star formation activity significantly decreases resulting in slow increase until $\log(t_L) \approx 8.5$. There is no discernible increase in cSFH due to the almost complete quenching of star formation from $\log(t_L) \approx 8.5$.

The cSFH of dEs is very similar to that of dS0s, while there is a significant difference in the cSFH of dSphs. Seo & Ann (2023) examined the SFHs of dSph and dE galaxies and conclude that the significant difference between dSphs and dEs is related to the origin of these galaxies. The dSph galaxies are thought to be originated from the primordial galaxies while dE galaxies, at least significant fraction of them, are transformed from late-type galaxies. The similarity between dS0s and dEs suggests that dS0s are also likely to be transformed from late-type galaxies. The morphological properties which are characterised by the presence of central lens component strongly supports the transformation origin of dS0 galaxies. It is worth to note that, VCC (Binggeli et al. 1985) and EVCC (Kim et al. 2014) do not distinguish dSphs from dEs. In contrast, as shown in Figure 7, the cSFHs of these two types

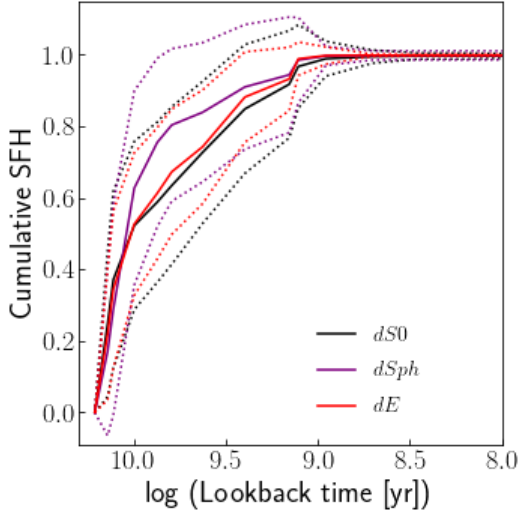


Figure 7. Mean cSFHs of dS0s compared with those of dEs and dSphs. Solid lines represent the mean cSFHs and dotted lines designate $\pm 1\sigma$ boundaries.

are significantly different. The similarity in cSFHs of dS0s and dEs suggests potential commonalities in their evolutionary processes and histories. This similarity and difference in the cSFHs of three sub-types of early-type dwarfs may provide insights into the formation and evolution of early-type dwarf galaxies within the broader context of galaxy evolution.

4.2 Dependence on Physical and Environmental Properties

4.2.1 Morphology

There are two distinct morphological features associated with dS0 galaxies, outer spiral arms and nucleation. Outer spiral arms are unique features observed specifically in dS0 galaxies, while nucleation is a common trait among early-type dwarfs. Despite nucleation being a prevalent characteristic in early-type dwarfs (encompassing dS0s, dEs, and dSphs), the fraction of nucleated dS0 galaxies is notably smaller than that of dEs and dSphs, both of which exhibit nucleation in $\sim 85\%$ of their populations. This discrepancy is likely due to the presence of the central lens component, which distinguishes dS0 galaxies as a distinct sub-type within the category of early-type dwarfs. The fraction of dS0 galaxies that possess outer spiral arms is 0.2.

Figure 8 illustrates the mean cSFHs of dS0 galaxies as a function of lookback time, categorized based on the presence or absence of outer spiral arms and nucleation. In CVCG, galaxies with outer spiral arms are classified as dS0_p, while those with nucleation are labeled as dS0_n. In the left panel of Figure 8, we present the mean cSFHs of these 30 dS0_p galaxies along with the 118 remaining dS0 galaxies obtained via 3σ clipping. The analysis reveals no significant difference in the cSFHs between dS0_p galaxies and dS0 galaxies, with only a marginal difference between the two samples noted between $\log(t_L) = 10$ and $\log(t_L) = 9.4$. Given the lack of significant differences between the cSFHs of dS0_p galaxies and dS0 galaxies, we combine the two samples and refer to them collectively as dS0s for subsequent analysis.

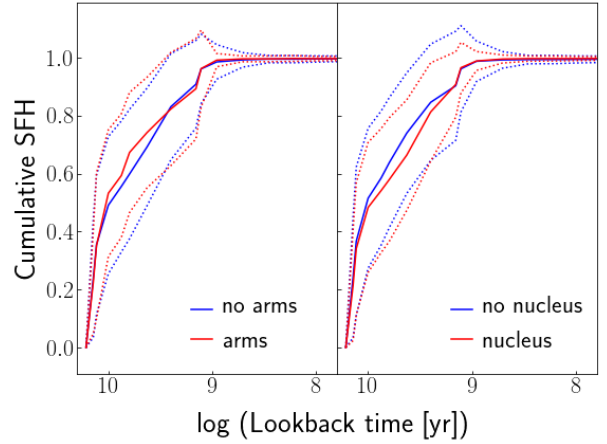


Figure 8. Mean cSFHs of early-type dwarfs with and without spiral arms (left panel) and nucleation (right panel). The line styles are the same as those in Figure 7.

Another important morphological characteristic that distinguishes early-type dwarf galaxies is the presence of nucleation. In the case of dwarf lenticular galaxies listed in Ann et al. (2015), $\sim 50\%$ of them exhibit nucleation, with significant variations in size and brightness observed among these galaxies. In the right panel of Figure 8, we present the mean cSFHs of dS0 galaxies, divided into those with and without nucleation. Similar to the cSFHs of dS0 galaxies categorized by the presence or absence of spiral arm features, the cSFHs of dS0 galaxies with and without nucleation are quite similar. However, a slightly more rapid star formation phase is observed between $\log(t_L) \approx 10$ and $\log(t_L) \approx 9$ in the cSFH of dS0 galaxies that lack nucleation.

The analysis reveals only a slight difference in cSFHs between $\log(t_L) \approx 10$ and $\log(t_L) \approx 9$. Consequently, the presence or absence of additional morphological features, such as outer spiral arms and nucleation does not significantly influence the cSFHs of dS0 galaxies.

4.2.2 Stellar Mass

We determined the stellar mass of a galaxy from the model flux fitted by STARLIGHT by using the galaxy distance in the CVCG. Since the flux obtained through the 3'' fiber which covers a small fraction of a galaxy image, we applied an aperture correction (AC) calculated as

$$AC = \frac{2 \times \int_0^{R_e} 2\pi f(r) r dr}{\int_0^{R_f} 2\pi f(r) r dr} \quad (4)$$

where R_e and R_f are the effective radius and the fiber radius, respectively, and $f(r)$ is the Sérsic profile (Sérsic 1968). We assumed an axis-symmetric luminosity distribution and used the fact that the luminosity within R_e is half of the total luminosity. We use the R_e and Sérsic index (n) that were determined by Seo & Ann (2022). For galaxies with unknown R_e and n , we use the mean R_e and n derived for dS0s. The number of galaxies with unknown Sérsic parameters is $\sim 10\%$ of the sample galaxies. The stellar masses of dS0 galaxies were found to fall within the range of $\sim 5 \times 10^6 M_\odot$ to $\sim 10^{10} M_\odot$.

Figure 9 shows a comparison between the present estimates

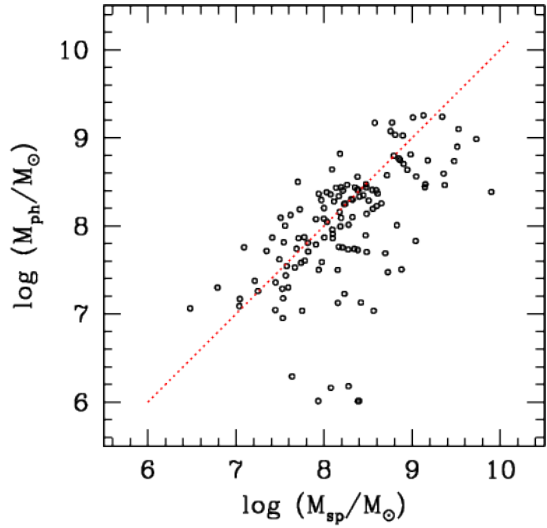


Figure 9. Comparision between stellar masses derived in this study and those from photometry based on SDSS DR12. One-to-one relation is give by a red dotted line.

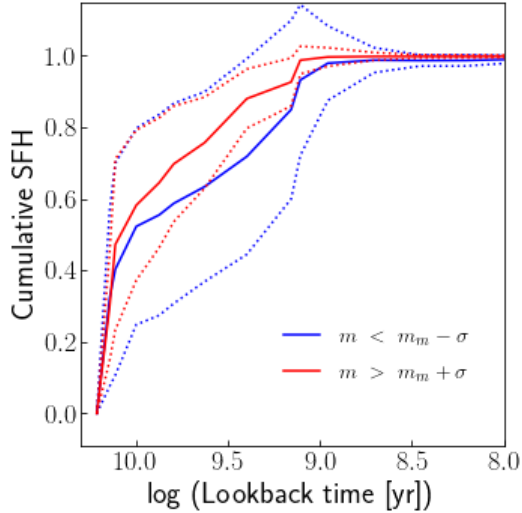


Figure 10. Mean cSFHs of dS0s grouped by stellar mass with $\pm 1\sigma$ envelopes. Galaxies in the lower mass group have stellar mass smaller than the median mass $- \sigma$ while those in the high mass group have stellar mass larger than the median mass $+ \sigma$. The line styles are the same as those in Figure 7.

of the total stellar mass and those from SDSS DR12. The total stellar masses provided by SDSS DR12 were derived from multi-band photometric images following Kauffmann et al. (2003) and Brinchmann et al. (2004). Approximately 10% of the sample galaxies are missing in the stellar mass table of SDSS DR12. There is a strong correlation between the two sets of stellar masses. The tight correlation for the majority of sample galaxies is remarkable because the two approaches are completely independent.

Given the belief that the mass of a galaxy plays a crucial role in star formation, particularly in early-type dwarf galaxies, we divided the dS0 galaxies into two groups based on their stellar mass. The high mass group comprises the dS0

galaxies with stellar masses greater than the median mass plus one standard deviation (σ), while the low mass group includes the dS0 galaxies with stellar masses smaller than the median mass minus one standard deviation (σ).

In Figure 10, we present the mean cSFHs of dS0 galaxies along with the 1σ boundaries, segregated into these two groups, as a function of lookback time. We calculated the mean cSFHs by applying 3σ clipping. As depicted in Figure 10, the cSFHs of dS0 galaxies exhibit significant differences when grouped by stellar mass. The average cSFH of the high mass group shows a more rapid increase compared to that of the low mass group. Notably, the cSFH of the low mass group lies outside the 1σ boundary of the high mass group for lookback times between $\log(t_L) \approx 9.5$ and $\log(t_L) \approx 9.2$. This suggests a strong stellar mass dependence in the cSFHs of dS0 galaxies, which appears to be slightly more pronounced than the dependencies observed in dSphs and dEs, as reported in Seo & Ann (2023).

4.2.3 Colors

The selection of u-r colors as a representative color parameter for galaxies is based on the understanding that, among the various colors defined in the SDSS photometric system, u-r colors are most closely linked to the SFHs of galaxies. In Figure 11, we present the cSFHs of dS0 galaxies, categorized by their u-r colors. Similar to our approach for stellar mass, we divided galaxies into two color groups using the median and standard deviation (σ) of u-r colors. Galaxies with u-r colors falling below the median minus σ were placed in the "blue" color group, while those with u-r colors exceeding the median plus σ were classified as "red" galaxies.

As depicted in Figure 11, there is a substantial difference in the cSFHs of the two color groups. Once again, the mean cSFH of blue dS0 galaxies lies outside the 1σ boundary of the cSFHs of red dS0 galaxies. After the earliest period of star formation, red galaxies exhibit a more rapid formation of stars compared to blue galaxies. Red galaxies conclude their star formation before a lookback time of $\log(t_L) = 9.2$, while blue galaxies continue forming stars until $\log(t_L) = 8$. This suggests that the red colors observed in some dS0 galaxies are a result of the early quenching of star formation. The strong color dependence of cSFHs in dS0 galaxies appears to be a natural consequence, as star formation significantly influences the colors of galaxies.

4.2.4 Background density

The SFHs of galaxies are known to be influenced by their environment (e.g., Kauffmann et al. 2004). In this study, we employed the background density (Σ) as a measure of galaxy environment. There are several methods to calculate background density (see Muldrew et al. 2012, for details), but for this analysis, we utilized the n -th nearest neighbor method with $n = 5$. This method necessitates two constraints for selecting neighboring galaxies: the linking velocity (ΔV^*) and the limiting magnitude (M_{lim}). We set the linking velocity ΔV^* to be 500 km s^{-1} and the limiting magnitude as $M_r = -15.2$ for local effect and $M_r = -20.6$ for global effect. They are the r-band absolute magnitudes. The former corresponds to the luminosity to define a volume-limited sample

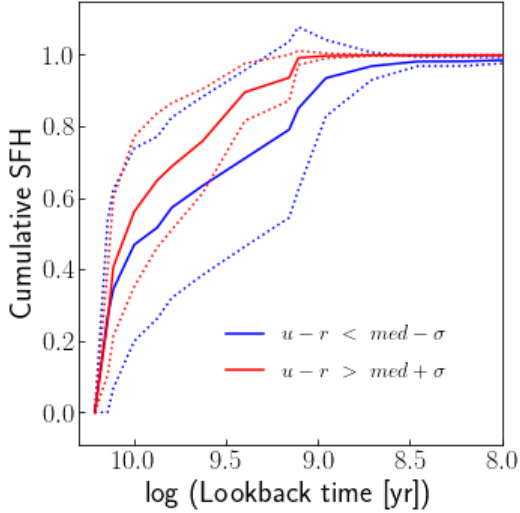


Figure 11. Mean cSFHs of dS0s grouped by u-r color. Galaxies in the blue color group have u-r colors smaller than the median u-r color $-\sigma$, while those in the red color group have u-r colors larger than the median $+\sigma$. The line styles are the same as those in Figure 7.

for galaxies with redshifts less than $z = 0.01$ and the latter is the M^* defined in the luminosity function of the local universe (Ann et al. 2015).

We calculated the background density Σ using the following equation,

$$\Sigma = \frac{n}{\pi r_p^2} \quad (5)$$

where r_p is the projected distance to the n th nearest neighbor galaxy. We normalized Σ using the mean background density ($\bar{\Sigma}$) of the galaxies in the local universe within $z = 0.01$. In the calculation of Σ , we utilized the galaxy distances from the CVCG.

Figure 12 presents the cSFHs of dS0 galaxies grouped by their background density (Σ). Similar to the approach used for physical parameters, we divided the galaxies into two groups based on the median and standard deviation (σ) of the background density. The low density group consists of galaxies with $\Sigma < \Sigma_m - \sigma$, while the high density group includes galaxies with $\Sigma > \Sigma_m + \sigma$, where Σ_m represents the median of the background density and σ is the standard deviation.

It is apparent that a distinction exists between the two groups in their cSFHs when grouped by background density, as constrained by $M_r = -15.2$. However, there is not a substantial difference observed for the two groups constrained by $M_r = -20.6$. This suggests that star formation in dS0 galaxies is likely more influenced by the local environment than by the global environment associated with large-scale structures. It is worth noting that the differences observed in the upper panel are statistically insignificant as the cSFHs fall within the 1σ boundary. The most pronounced difference in the cSFHs of the two density groups occurs around $\log(t_L) = 9.3$.

During the second period of star formation, where intermediate-age stellar populations play a significant role, the background density appears to have a more pronounced

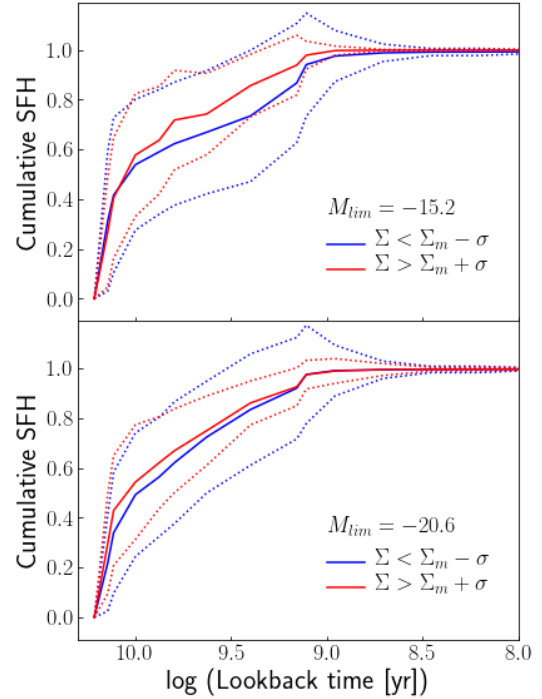


Figure 12. Mean cSFHs of dS0s grouped by the background density. We present the background density constrained by $M_{lim} = -15.2$ in the upper panel and that with $M_{lim} = -20.6$ in the lower panel. We plot the mean values with their $\pm 1\sigma$ envelopes for each group. Group division was made by the median and σ of the background density. The line styles are the same as those in Figure 7.

impact. High-density regions are more likely to witness star formation during this phase. It's important to note that the stars formed during the second period of star formation do not originate from primordial gas but rather from enriched gas that has been ejected and subsequently falls back into the galaxy after a period of highly reduced star formation. In this scenario, a denser environment may be advantageous in retaining the ejected gas for a longer duration, thereby facilitating its involvement in subsequent star formation episodes.

4.3 Quenching Epoch

Figure 13 displays the frequency distribution of quenching time (τ_{90}) for 148 dS0 galaxies categorized by the presence of spiral arm features and nucleation. The term quenching time (τ_{90}) was introduced by Weisz et al. (2014a,b, 2019) to quantify the cSFH of galaxies. It is defined as the lookback time at which 90% of the stellar mass has formed. The overall characteristics of the τ_{90} distribution resemble a Gaussian distribution with tails extending towards both the low and high ends. In particular, $\sim 10\%$ of dS0 galaxies exhibit τ_{90} greater than the lookback time of 10 Gyr. Similar distributions have also been observed in dSphs and dEs, with a higher fraction in dSphs (Seo & Ann 2023).

As elucidated by Seo & Ann (2023), the extremely early quenching of early-type dwarf galaxies is likely due to their small mass, as low-mass galaxies are known to undergo quenching at earlier stages (Digby et al. 2019; Garrison-Kimmel et al. 2019; Joshi et al. 2021). It appears highly prob-

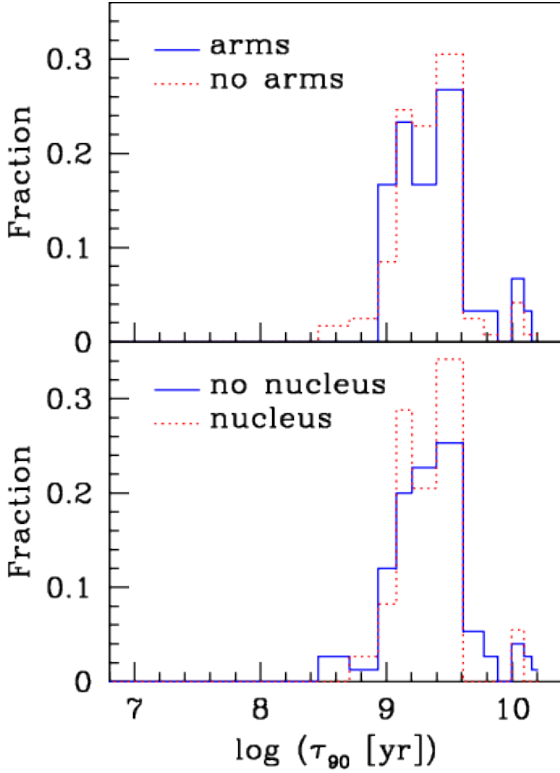


Figure 13. Frequency distributions of quenching time τ_{90} . The upper panel shows the quenching times grouped by outer spiral arms, while the lower panel shows the quenching times grouped by nucleation.

able that dS0 galaxies with τ_{90} greater than the lookback time of 10 Gyr represent genuine primordial objects. The scarcity of such early-quenched dS0 galaxies suggests that the majority of dS0 galaxies may not be primordial in nature.

As anticipated due to the slight variations in the SFHs of dS0 galaxies with different morphological properties, there are discernible differences in τ_{90} values among dS0 galaxies with distinct morphologies. Concerning the presence of spiral arm features, no dS0 galaxies with spiral arms exhibit $\log(\tau_{90})$ smaller than 9, while a small fraction of dS0 galaxies without spiral arms quenched at $\log(\tau_{90}) < 9$. In contrast, there is no notable distinction in late quenching between dS0 galaxies with and without nucleation. It's worth noting that the distribution of τ_{90} values appears somewhat narrower in dS0 galaxies with nucleation compared to those without nucleation, particularly when we disregard the high-end tail.

5 DISCUSSION AND CONCLUSIONS

In this study, we analyzed SDSS spectra to determine the star formation histories (SFHs) of 148 dS0 galaxies. To achieve this, we employed the population synthesis code STARLIGHT (Cid Fernandes et al. 2005). Our investigation has unveiled distinct characteristics within the SFHs of dS0 galaxies. At a lookback time of ~ 14 Gyr, these galaxies underwent an initial explosive starburst, followed by subsequent bursts of star formation peaking at a lookback time of 10 Gyr and 2.5 Gyr. The peak occurring at a lookback

time of ~ 10 Gyr primarily consists of older, metal-poor stars, while the peak at a lookback time of 2.5 Gyr predominantly comprises intermediate-metallicity stars. Notably, extremely metal-poor ($Z=0.0001$) stars are relatively rare during the early stages of galaxy formation, suggesting possible pre-enrichment influenced by Population III stars during the re-ionization period.

Furthermore, our investigation suggests that stellar feedback plays a pivotal role in the early cessation of star formation in many dS0s, resulting in gaps in their SFHs. This early quenching effect is also observed in dSphs and dEs (Seo & Ann 2023). Among the three types of early-type dwarfs, early quenching is most pronounced in dSphs, while dS0s exhibit an intermediate between dSphs and dEs.

The star formation activity within dS0 galaxies can be categorized into three distinct periods. The first period exhibits two prominent peaks, one at a lookback time of ~ 14 Gyr and the other at a lookback time of 10 Gyr. The former marks the onset of an explosive starburst phase, contributing approximately 25% to the present-day stellar mass of dS0s. The latter epoch is notable for the generation of a majority of metal-poor stars.

The second period spans from around the lookback time of 6.3 Gyr to 1 Gyr, with the bulk of star formation occurring around the lookback time of 2.5 Gyr. This phase predominantly gives rise to intermediate-metallicity stars. In dS0s, the stellar mass produced at the peak of the second period is comparable to that generated at the second peak of the first period. In the second period of star formation, the level of star formation activity is comparatively lower than that observed in the first period. However, stars with intermediate metallicity formed around the peak of the second period contribute $\sim 30\%$ of the current stellar mass. This substantial contribution is attributed to the stars formed during the peak of the second period of star formation. The third period of star formation recommences around the lookback times of 0.1 Gyr after a phase of quiescent star formation. However, its contribution to the current stellar mass is deemed negligible.

We have undertaken an investigation into the cSFHs of dS0 galaxies, taking into account various factors including morphology, stellar mass, u-r color, and background density. The cSFHs of dS0 galaxies reveal discernible dependencies on two crucial physical properties: stellar mass and u-r color. Notably, u-r color exerts a substantial influence on cSFHs. Conversely, the presence or absence of morphological features such as outer spiral arms and nucleation at the nuclei does not exhibit statistical significance. Additionally, while cSFHs in dS0 galaxies appear to evolve more rapidly in high-density areas, this correlation does not achieve statistical significance.

The absence of significant dependence of cSFHs on morphological features, the outer spiral arms and nucleation, particularly during the early stages of galaxy formation, suggests that these morphological traits likely emerged after the initial period of star formation. This interpretation is supported by the observed differences in cSFHs that occur after the lookback time of 10 Gyr. Furthermore, it is plausible that the outer spiral arms have minimal influence on star formation in the central regions of these galaxies, as these features are typically located outside the central star-forming regions.

While the dependence of cSFHs on the background density (Σ) in dS0 galaxies is weaker compared to the influence of stellar mass, it is still a significant factor to consider. This

is because some dS0 galaxies are likely the result of transformations from late-type galaxies, and morphology transformations are often driven by interactions with the environment. One indicator of this transformation is the presence of embedded structures in dS0 galaxies, reminiscent of late-type galaxies. A similar situation is observed in dEs, where a notable fraction of them also possess embedded disc features (Seo & Ann 2022). It is not clear but we suggest that the presence of a second peak in the SFHs of dS0 galaxies and dEs is related to this morphology transformation. However, a substantial fraction of dS0s display early quenching, characterized by τ_{90} greater than a lookback time of 10 Gyr, suggesting their primordial origin. In contrast, dSph galaxies, which are mostly considered primordial objects, lack this second peak in their SFHs.

The almost absence of extremely metal-poor ($Z = 0.0001$) stars in dS0 galaxies suggests the possibility of pre-enrichment of the gas from which these galaxies formed. This interpretation aligns with previous findings by Seo & Ann (2023), who proposed that the lack of extremely metal-poor stars in dEs and dSphs could be attributed to the rapid enrichment of metals by supernovae from Population III stars. This absence of extremely metal-poor stars is consistent with observations of metallicity in various astrophysical environments, including the Milky Way halo stars, local group dwarf spheroidal galaxies (Helmi et al., 2006), damped Ly α absorption systems (Wolfe et al., 1998), and intervening intergalactic medium along sightlines to quasars (Cowie et al., 1998). The general absence of extremely metal-poor stars in the oldest stellar populations strongly suggests that the gases from which these stars formed were pre-enriched. This pre-enrichment, which resulted in the metallicity of the oldest stars reaching as high as $Z = 0.0004$, is consistent with numerical simulations (Tornatore et al., 2012; Wise et al., 2012) demonstrating the production of metals by Population III supernovae.

ACKNOWLEDGEMENTS

H. B. Ann thanks Dr. Roberto Cid Fernandes for sending the source code of STARLIGHT.

DATA AVAILABILITY

The original data underlying this article are available in the SDSS DR7. Additional data are available upon request.

REFERENCES

Aguerri J. A. L., Iglesias-Páramo J., Vílchez J. M., Muñoz-Tuñón C., Sánchez-Janssen R., AJ, 130, 475

Ann H. B., Seo M., Ha D. K., 2015, ApJS, 217, 27

Ann H. B., 2017, JKAS, 50, 111

Barazza F. D., Binggeli B., Jerjen H., 2002, A&A, 391, 823

Barazza F. D., Binggeli B., Jerjen H., 2003 A&A, 407, 121

Binggeli B., Cameron L. M., 1991, A&A, 252, 27

Binggeli B., & Cameron L. M., 1993, A&AS98, 297

Binggeli B., Sandage A., Tammann G. A. 1985, AJ, 90, 1681

Boselli A., Boissier S., Cortese L., Gavazzi G., 2008, ApJ, 674, 742

Boselli A., Fossati M., Sun M., 2022, The Astronomy and Astrophysics Review, 30, 3

Brinchmann J., Charlot S., Whitw S. D., Tremoni C., Kauffmann G., Hexkman T., Brinkmann J., 2004, MNRAS, 351, 1151

Bruzual G., Charlot S., 2003, MNRAS, 344, 1000

Buta R. J., 2013, in Planets, Stars and Stellar Systems, vol 6, ed. Terry D. Oswalt, & Willuam, C. Keel (New York: Springer Science+Business Media Dordrechr), 1

Cappellari M., 2017, MNRAS, 466, 798

Cappellari M., Emsellem E., 2004, PASP, 116, 138

Chilingarian I., Cayatte V., Revaz Y., Dodonov S., Durand D., Durret F., Micol A., Slezak E., 2009, Sci, 326, 1379

Cid Fernandes, R., Gonzalez. D. R. M., Schmitt, H., Storchi-Bergmann, T., Martins, L. P., Perez, E., Heckman, T., Leitherer, C., Schaerer, D., ApJ, 605, 105

Cid Fernandes R. et al., 2005, MNRAS, 358, 363

Cid Fernandes R., 2018, MNRAS, 480, 4480

Cowie L. L., Songaila A., Hu E. M., Cohen J. G., 1996, AJ, 112, 839

Daddi E. et al., 2007, ApJ, 670, 156

De Rijcke S., Dejonghe H., Zeilinger W. W., Hau G. K. T., 2003, A&A, 119, 125

De Lucia G. et al., 2007, MNRAS, 374, 809

Digby R. et al., 2019, MNRAS, 485, 5423

Dressler A., 1980, ApJ, 236, 351

Ferrarese L. et al., 2006, ApJS, 164, 33

Garrison-Kimmel, S. et al., 2019, MNRAS, 489, 4574

Gavazzi G., Boselli A., Cortese L., Arosio I., Gallazzi A., Pedotti P., Carrasco L., 2006, A&A, 446, 839

Graham A. W., Guzman R., 2003, AJ 125, 2936

Graham A. W., Janz J., Penny S. J., Chilingarian I. V., Ciambur B. C., Forbes D. A., Davies R. L., 2017, ApJ, 840, 68

Graham A. W., Jerjen H., Guzman R., 2003, AJ, 126, 1787

Gunn J. E., Gott III J. R., 1972, ApJ, 176, 1

Janz J. et al., 2012, ApJ, 745, L24

Janz J. et al., 2014, ApJ, 786, 105

Jerjen H., Kalnajs A., Binggeli B., 2000, A&A, 358, 849

Jerjen H., Kalnajs A., Binggeli B., 2001, in Funes J. G., Corsini E. M., eds, ASP Conf. Ser. Vol. 230, Galaxy Disks and Disk Galaxies. Astron. Soc. Pac., San Francisco, p.239

Joshi G. D., Pillepich A.r, Nelson, D., Zinger, E., Marinacci, F., Springel V., Vogelsberger M., Hernquist L., 2021, MNRAS, 508, 1652

Kauffmann G. et al., 2003, MNRAS, 341, 54

Kauffmann G. et al., 2004, MNRAS, 353, 713

Kim, S. et al., 2014, ApJS, 215, 22

Le Borgne J.-F. et al., 2003, A&A, 402, 433

Lisker T., Grebel E. K., Binggeli B., 2006, AJ, 132, 497

Lisker T., Grebel E. K., Binggeli B., Glatt K., 2007, ApJ, 660, 1186

Lisker T., Fuchs B., 2009, A&A, 501, 429

Magris C. Gladis, Mateu P. Juan, Mateu C., Bruzual A. Gustavo, Cabrera-Ziri I., Mejía-Narváez A., PASP, 127, 16

Makarov D. I., Karachentsev I., 2011, MNRAS, 412, 2498

Moore B., Katz N., Lake G., Dressler A., Oemler A., 1996, Nature, 379, 613

Moore B., Lake G., Katz N., 1998, ApJ, 495, 139

Muldrew S. I. et al., MNRAS, 419, 2670

Noeske, K. H. et al., 2007, ApJ, 660, L43

Oemler A. Jr., 1974, ApJ, 194, 1

Peng C. Y., Ho L. C., Impey C. D., Rix H. -W., 2010, AJ, 139, 2097

Penny S. J., Forbes D. A., Pimbblet K. A., Floyd D. J. E., 2014, MNRAS, 443, 3381

Pérez-Millán D. et al., 2023, MNRAS, 521, 1292

Reyden B. S., Terndrup D. M., Pogge R.W., Lauer T. R., 1999, ApJ, 517, 650

Riffel R. et al., 2021, MNRAS, 501, 4064

Rodighiero G. et al., 2011, ApJ, 739, L40

Salim S. et al., 2007, ApJS, 173, 267

Sánchez-BLázquez P. et al., 2009, *A&A*, 499, 47
 Sandage A., Bibgeli B., 1984, *AJ*, 89, 919
 Seo M., Ann H. B., 2022, *MNRAS*, 514, 5853
 Seo M., Ann H. B., 2023, *MNRAS*, 520, 5521
 Sérsic J. L., 1968, *Atlas de Galaxias Australes* (Cordoba: Observatorio Astronomico)
 Smith R., Fellhauer M., Assmann P., 2012, *MNRAS*, 420, 1990
 Sobral D., Best P. N., Small I., Mobasher B., Stott J., Nisbet D., 2014, *MNRAS*, 437, 3516
 Speagle J. S., Steinhardt C. I., Capak P. L., Silverman J. D., 2014, *MNRAS*, 437, 3516
 Spitzer L. Jr., Baade W., 1951, *ApJ*, 113, 413
 Strateva I., et al., 2001, *AJ*, 122, 1861
 Steyrleithner P., Hensler G., Boselli A., 2020, *MNRAS*, 494, 1114
 Tolstoy E., Hill V., Tosi M., 2009, *ARA&A*, 47, 371
 Wang B., 2022, *MNRAS*, 516, 429
 Weisz D. R., Dolphin A. E., Skillman E. D., Holtzman J., Gilbert K. M., Dalcanton J. J., Williams B. F., 2014a, *ApJ*, 789, 147
 Weisz D. R., Dolphin A. E., Skillman E. D., Holtzman J., Gilbert K. M., Dalcanton J. J., Williams B. F., 2014b, *ApJ*, 789, 148
 Weisz D. R., Dolphin A. E., Skillman E. D., Holtzman J., Gilbert K. M., Dalcanton J. J., Williams B. F., 2015, *ApJ*, 804, 136
 York D. G. et al., 2000, *AJ*, 120, 1579

This paper has been typeset from a TeX/LaTeX file prepared by the author.